

A NEW DENSITY VARIANCE - MACH NUMBER RELATION FOR SUBSONIC AND SUPERSONIC, ISOTHERMAL TURBULENCE

KONSTANDIN, L.^{1,2}, GIRICHIDIS, P.^{1,2,3,4}, FEDERRATH, C.^{1,5}, KLESSEN, R. S.¹

draft October 8, 2018

ABSTRACT

The probability density function (PDF) of the gas density in subsonic and supersonic, isothermal, driven turbulence is analysed with a systematic set of hydrodynamical grid simulations with resolutions up to 1024^3 cells. We performed a series of numerical experiments with root mean square (r.m.s.) Mach number \mathcal{M} ranging from the nearly incompressible, subsonic ($\mathcal{M} = 0.1$) to the highly compressible, supersonic ($\mathcal{M} = 15$) regime. We study the influence of two extreme cases for the driving mechanism by applying a purely solenoidal (divergence-free) and a purely compressive (curl-free) forcing field to drive the turbulence. We find that our measurements fit the linear relation between the r.m.s. Mach number and the standard deviation of the density distribution in a wide range of Mach numbers, where the proportionality constant depends on the type of the forcing. In addition, we propose a new linear relation between the standard deviation of the density distribution σ_ρ and the standard deviation of the velocity in compressible modes, i.e. the compressible component of the r.m.s. Mach number $\mathcal{M}_{\text{comp}}$. In this relation the influence of the forcing is significantly reduced, suggesting a linear relation between σ_ρ and $\mathcal{M}_{\text{comp}}$, independent of the forcing, ranging from the subsonic to the supersonic regime.

Subject headings: compressible turbulence

1. INTRODUCTION

Understanding the intricate interplay between interstellar turbulence and self-gravity is one of the key problems in star formation theory. The supersonic turbulent velocity field is likely responsible for the complex and filamentary density structures observed in molecular clouds. It creates dense regions that can become gravitationally unstable and collapse into dense cores and eventually turn into new stars (Elmegreen & Scalo 2004; Mac Low & Klessen 2004; McKee & Ostriker 2007). Statistical quantities, describing this process, such as the initial mass function, the core mass function (Padoan & Nordlund 2002; Hennebelle & Chabrier 2008, 2009), and the star formation rate (Hennebelle & Chabrier 2011; Padoan & Nordlund 2011) depend on the standard deviation (std. dev.) of the density of the molecular cloud. The pioneering works by Padoan et al. (1997) and Passot & Vázquez-Semadeni (1998) have shown that the std. dev. σ_ρ of the probability density function (PDF) of

the mass-density grows proportional to the root mean square (r.m.s.) Mach number \mathcal{M} of the turbulent flow

$$\sigma_\rho / \langle \rho \rangle_V = b \mathcal{M}, \quad (1)$$

where $\langle \rho \rangle_V$ is the volume-weighted mean density and b is a proportionality constant. Federrath et al. (2008, 2010) explained the dependence of σ_ρ on b by taking the modes of the forcing into account that drive the turbulent velocity field. This model predicts for purely solenoidal forcing $b = 1/3$ and for purely compressive forcing $b = 1$, and explains the large deviations of b ranging from $b = 0.26$ to $b = 1.05$ in previous works (e.g. Padoan et al. 1997; Passot & Vázquez-Semadeni 1998; Li et al. 2003; Kritsuk et al. 2007; Beetz et al. 2008; Schmidt et al. 2009; Price et al. 2011; Konstandin et al. 2012; Molina et al. 2012). We follow up on this work and discuss the physical origin of this dependency and introduce a new relation, similar to equation (1), however, correlating the compressible component of the r.m.s. Mach number $\mathcal{M}_{\text{comp}}$ with σ_ρ .

In section 2 we explain our numerical setup. We analyse the influence of measuring mass-weighted and volume-weighted distributions in section 3.1, the influence of the resolution on our measurements in section 3.2 and the PDFs of the mass density and the compressible part of the velocity field in section 3.3. In section 3.4, we present the linear relations between the std. dev. of the mass density and the r.m.s. Mach number. In section 3.5 we discuss the new relation between the std. dev. of the mass density and the std. dev. of the compressible part of the velocity field. A summary of our results and conclusions is given in section 4.

2. SIMULATIONS AND METHODS

We use the piecewise parabolic method (Colella & Woodward 1984) implemented in the grid code FLASH3 (Fryxell et al. 2000; Dubey et al.

email: konstandin@stud.uni-heidelberg.de

¹Zentrum für Astronomie der Universität Heidelberg, Institut für Theoretische Astrophysik, Albert-Ueberle-Str.2, D-69120 Heidelberg, Germany

²Member of the International Max Planck Research School for Astronomy and Cosmic Physics at the University of Heidelberg (IMPRS-HD) and the Heidelberg Graduate School of Fundamental Physics (HGSFP).

³Max Planck Institut für Astrophysik, Karl-Schwarzschild-Str. 1, 85741 Garching, Germany

⁴Hamburger Sternwarte, Gojenbergsweg 112, 21029 Hamburg, Germany

⁵Monash Centre for Astrophysics (MoCA), School of Mathematical Sciences, Monash University, Vic 3800, Australia

2008) to solve the hydrodynamical equations on a uniform three-dimensional grid. These equations are the continuity equation

$$\frac{\partial \rho}{\partial t} + (\mathbf{v} \cdot \nabla) \rho = -\rho \nabla \cdot \mathbf{v}, \quad (2)$$

the Euler equation with a stochastic forcing term \mathbf{F} per unit mass

$$\frac{\partial \mathbf{v}}{\partial t} + (\mathbf{v} \cdot \nabla) \mathbf{v} = -\frac{\nabla p}{\rho} + \mathbf{F}, \quad (3)$$

and the equation of state

$$p = \kappa \rho^\Gamma, \quad (4)$$

where \mathbf{v} is the velocity field, $s = \ln(\rho / \langle \rho \rangle_V)$ is the natural logarithm of the mass density ρ , c_s is the sound speed, p the pressure, Γ the adiabatic index. Since isothermal gas is assumed throughout this study, $\Gamma = 1$, the pressure, $p = \rho c_s^2$, is proportional to the mass density with a fixed sound speed c_s . These simulations are scale free, so we set $\langle \rho \rangle_V = 1$, $c_s = 1$, and the box size of the simulation $L = 1$. The numerical simulations are evolved for ten dynamical time scales $T = L / (2\mathcal{M}c_s)$, where $\mathcal{M} = v_{r.m.s.} / c_s$ is the r.m.s. Mach number of the simulations with the r.m.s. velocity $v_{r.m.s.}$. All relevant quantities are stored in intervals of $0.1T$. The stochastic forcing field \mathbf{F} has an autocorrelation time equal to the dynamical time scale on the injection scale, and varies smoothly in space and time. The forcing field is constructed in Fourier space such that the kinetic energy is injected on the largest scales, where $1 < kL/2\pi < 3$. To analyse the influence of different modes of the forcing field, we use projection tensors in Fourier space to get a purely divergence-free, $\nabla \cdot \mathbf{F} = 0$, solenoidal or a purely curl-free, $\nabla \times \mathbf{F} = 0$, compressive vector field for the forcing. We adjust the amplitude of the forcing, such that we have r.m.s. Mach numbers $\mathcal{M} = 0.1, 0.5, 2, 5.5, 15$ for both types of forcing in the stationary state of fully developed turbulence. To investigate the effects of numerical viscosity, we study simulations at different resolutions, 128^3 , 256^3 , 512^3 and 1024^3 . The parameters of these simulations are described in Konstandin et al. (2012), and a detailed description of the forcing is presented in Schmidt et al. (2009) and Federrath et al. (2010).

3. RESULTS

Figure 1 shows the time evolution of the r.m.s. Mach numbers \mathcal{M} in all simulations. The fluid reaches the equilibrium state of fully developed turbulence after about two turbulent crossing times $t \approx 2T$. We thus average all the following analyses for $2 \leq t/T$.

3.1. Volume-weighted and mass-weighted probability density functions

It is well-known that the PDF of the logarithm of the mass density $p(s)$ in a turbulent, isothermal medium is close to a Gaussian distribution (see e.g. Vazquez-Semadeni 1994; Passot et al. 1994; Padoan et al. 1997; Klessen 2000; Kritsuk et al. 2007; Federrath et al. 2008; Konstandin et al. 2012)

$$p(s) = \frac{1}{\sqrt{2\pi}\sigma_s} \exp\left(-\frac{(s - \langle s \rangle)^2}{2\sigma_s^2}\right). \quad (5)$$

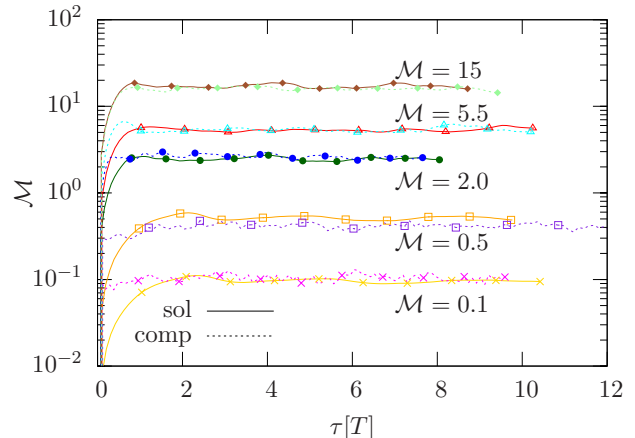


FIG. 1.— R.m.s. Mach number of all simulations as a function of the dynamical time scale, calculated by averaging over all grid cells for both types of forcing.

Li et al. (2003) showed with the assumption of a Gaussian, volume-weighted PDF of s that the mass-weighted PDF of s is also Gaussian with the same std. dev. and with a shifted mean value

$$\langle s \rangle_V = -\langle s \rangle_M = -\frac{\sigma_s^2}{2}. \quad (6)$$

Figure 2 shows the volume- and mass-weighted PDFs

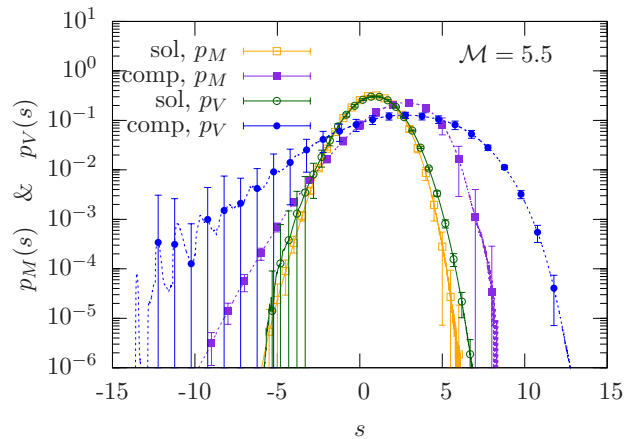


FIG. 2.— Mass-weighted and volume-weighted PDFs of the logarithm of the mass density in the simulations with $\mathcal{M} = 5.5$, 1024^3 grid cells and both types of forcing.

(the volume-weighted PDF is shifted with $\langle s \rangle_M - \langle s \rangle_V = \sigma_s^2$ for a better comparison) for the simulation with $\mathcal{M} = 5.5$ for both types of forcing. The PDFs are averaged over 81 time snapshots in the state of fully developed stationary turbulence for $t \geq 2T$ and the error bars indicate the std. dev. of the temporal fluctuations. The variance of the volume-weighted PDFs is larger than the variance of the mass-weighted distributions. This effect is stronger for the compressive forcing than for the solenoidal forcing. The volume-weighted PDFs show a larger variation with time in the low-density wing of the distribution than the mass-weighted distributions. This low-density wing also shows higher probabilities than one would expect from the underlying Gaussian distribution extrapolated from the high density wing. This effect is

stronger for the compressive than for the solenoidal forcing. We assume that this behaviour is caused by our forcing scheme. As the time correlation of the forcing field is equal to the dynamic time scale on the largest scales, the forcing has enough time to produce very low densities in large regions of diverging flows. This process causes the volume-weighted PDF of s to have a tail at low densities with higher probabilities than the distribution for the case of turbulence, which is not driven on the largest scales. With increasing r.m.s. Mach number and increasing amplitude of the forcing field this effect becomes more important and the low-density tail influences the calculated std. dev. of these distributions. This effect is less pronounced measuring the mass-weighted distributions, as the very low density grid cells carry only little mass. We note that there are other potential processes, which could lead to non-Gaussian wings in the PDF, such as turbulent intermittence (e. g. Klessen 2000).

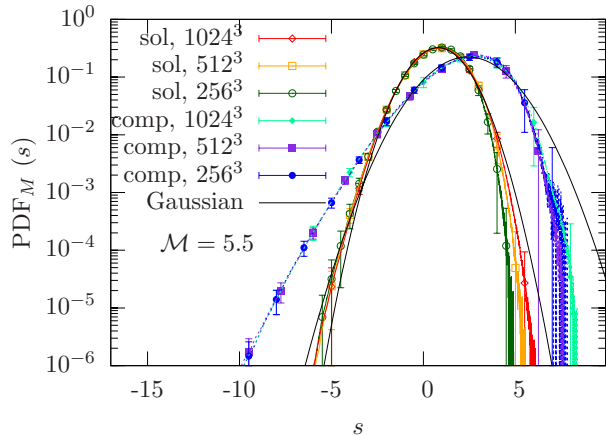


FIG. 3.— Mass-weighted PDFs of s of the simulations for $\mathcal{M} = 5.5$, different resolutions and both types of forcing. The black solid lines are Gaussian functions with mean value and std. dev. calculated with the highest resolution.

3.2. Resolution effects on the probability density functions

Figure 3 shows the mass-weighted PDF of the quantity s with an r.m.s. Mach number $\mathcal{M} = 5.5$ and different resolutions. The PDF of s shows deviations from the Gaussian shape and a dependency on the resolution only in the high-density tails of the distribution. We interpret the deviations of our measured PDFs from the Gaussian distribution in the supersonic regime for both types of forcing as a sign of numerical dissipation and finite sampling. In the highly supersonic regime the medium is dominated by shock fronts and high-density gradients, which require high resolution to converge. As we do not fully resolve them in the $\mathcal{M} = 5.5$ case, an additional dissipation occurs. This effect is stronger in the simulations with compressive forcing and becomes stronger with increasing r.m.s. Mach number for both types of forcing (not shown here). However, increasing the resolution has no influence on the deviations from the Gaussian distribution in the low-density tail of the mass-weighted PDFs.

With the assumption of a log-normally distributed

mass density, it can be shown that the std. dev. of the Gaussian-distributed quantity s is (see Price et al. 2011)

$$\sigma_s^2 = \ln(1 + \sigma_\rho^2). \quad (7)$$

Figure 4 shows σ_ρ as a function of σ_s for our volume-weighted (left panel) and mass-weighted (right panel) distributions. The volume- and the mass-weighted measurements of the std. dev. of s show increasing deviations from equation (7) with increasing r.m.s. Mach numbers for both types of forcing. However, the deviations are smaller in the mass-weighted case than in the volume-weighted one. The assumption of Gaussianity, which is implied in equation (7), is better fulfilled for the mass-weighted case. Figure 4 also shows that our measurements with $\mathcal{M} = 15$ are not converged with resolution for both types of forcing. Our measurements are in agreement with Price et al. (2011), who showed that direct measurements of σ_ρ show a stronger dependency on resolution than measurements of σ_s .

All volume-weighted measurements show a clear trend towards the relation (7) with increasing resolution. However, the data points do not fit relation (7) for $\mathcal{M} = 15$ with solenoidal forcing and in all the supersonic cases with compressive forcing, although the data points with $\mathcal{M} = 2$ and $\mathcal{M} = 5.5$ with compressive forcing are nearly converged with resolution. This can be explained with the non-Gaussian, low-density wing of the distributions, which does not depend on the resolution. Considering that the std. dev. $\sigma_{s,M}$ of the mass-weighted PDF is more compatible with the scaling for a log-normal PDF, equation (7), and that the resolution dependence of $\sigma_{s,M}$ is weaker than for $\sigma_{s,V}$, we prefer to use $\sigma_{s,M}$ as estimate for the turbulent density fluctuations in the following.

3.3. The probability density function of the density and of the compressible modes in the velocity field

Figure 5 shows the mass-weighted PDFs of the quantity s (left panels) and the volume-weighted PDFs of the compressible modes of the velocity field normalised to the sound speed $M_{\text{comp}} = v_{\text{comp}}/c_s$ (right panels) for different r.m.s. Mach numbers and both types of forcing. The PDFs of the logarithm of the density largely follow Gaussian distributions for all supersonic r.m.s. Mach numbers. We added Gaussian functions (black solid lines), with the first- and second-order moments calculated from our distributions in figure 5. The high-density tails of the distributions show deviations from the Gaussian shape, which increase with increasing r.m.s. Mach number. Also the deviations from the Gaussian distribution in the low-density tail, as discussed in section 3.1, get more pronounced with increasing r.m.s. Mach number. Thereby, we have large deviations of our measurement from the Gaussian distributions in the $\mathcal{M} = 15$ case and the calculated std. dev. does not correspond to the std. dev. of the underlying Gaussian distribution.

The density distributions of the simulations driven by solenoidal forcing in the subsonic regime show significant deviations from the log-normal shape, which become stronger as \mathcal{M} decreases. These distributions become more asymmetric and more peaked. The different behaviour of the PDFs in the subsonic regime especially for the solenoidal forcing is caused by the different physical

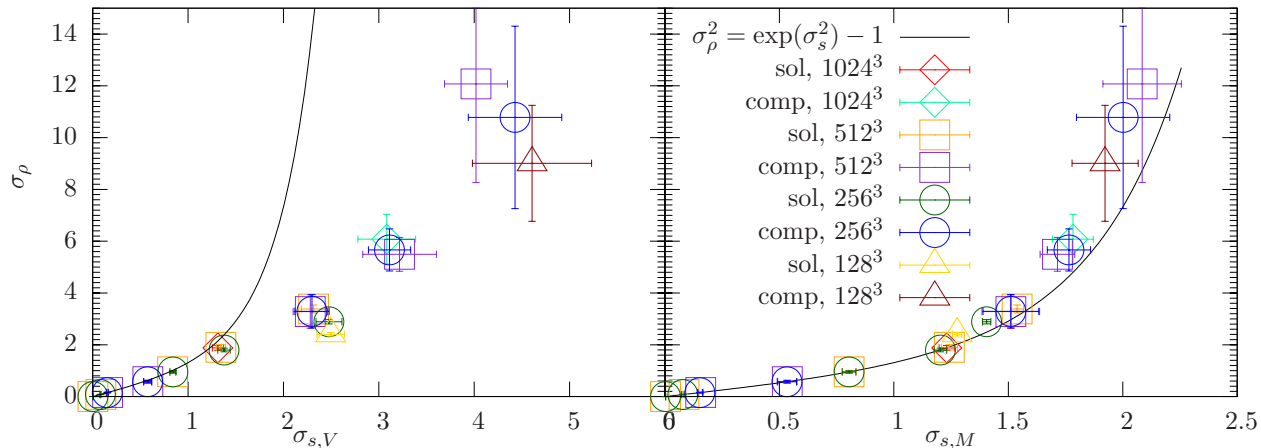


FIG. 4.— Std. dev. of the mass-density σ_ρ as a function of the std. dev. of the logarithm of the mass-density σ_s , measured volume-weighted (left panel) and mass-weighted (right panel). The deviations of the measurements from the black solid lines, equation (7), quantify the deviations from a log-normally distributed mass density.

processes acting here. In the subsonic regime sound waves transfer information faster than the averaged flow of the medium, such that the thermal pressure increases before two converging flows can collide. This process prevents colliding flows from producing high-density regions and causes the sharp edge at the high-density wing of the distributions. The thermal pressure also decelerates the velocities in compressible modes, such that the PDF of M_{comp} also shows a narrow, peaky and intermittent behaviour for the solenoidal forcing. This process is just visible for solenoidal forcing, because in the compressive forcing case the velocities in compressible modes are re-injected by the forcing to hold the r.m.s. Mach number constant. This is the reason why the thermal pressure does not have such a strong influence there.

The right panels of figure 5 show the PDFs of M_{comp} , where M_{comp} is calculated in Fourier space and averaged over the three directions of the coordinate system x, y, z in real space. The distributions of M_{comp} are symmetric with zero mean and have an increasing std. dev. with increasing r.m.s. Mach number. The distributions obtained with compressive forcing are always broader than with solenoidal forcing at the same r.m.s. Mach number. The PDFs of M_{comp} are Gaussian (black solid lines) with deviations in both wings. These are the signpost of turbulent intermittency. The deviations do not show a clear trend with the r.m.s. Mach number. The PDF of M_{comp} obtained with solenoidal forcing in the subsonic regime with $\mathcal{M} = 0.1$ shows the strongest deviations from the Gaussian shape with a narrow, peaky, intermittent distribution. These deviations are caused by the thermal pressure, as discussed above.

3.4. Relation between the r.m.s. Mach number and the standard deviation of the density

In Padoan et al. (1997) and Passot & Vázquez-Semadeni (1998) the authors found that the std. dev. of the PDF of the mass density σ_ρ is proportional to the r.m.s. Mach number in a turbulent flow. The std. dev. of the mass density is an important quantity especially in astrophysics, where the Mach

number dependency of density fluctuations is used to derive analytic expressions for the core mass function (CMF) and the stellar initial mass function (IMF) (e.g., Padoan & Nordlund 2002; Hennebelle & Chabrier 2008, 2009). On galactic scales it is used to reproduce the Kennicutt-Schmidt relation (Tassis 2007), and Elmegreen (2008) suggests that the star formation efficiency is a function of the density PDF. Figure 6 (upper left panel) shows the measured std. dev. of the mass density as a function of the r.m.s. Mach number for different resolutions and both types of forcing. The error bars in each panel of figure 6 indicate the std. dev. of the temporal fluctuations of the measured quantities. They do not include any potential systematic errors stemming from, e.g., the numerical scheme or implementation of the forcing algorithm. Thus, we interpret the error bars as a lower limit of the real uncertainty. The dotted and dashed-dotted lines correspond to the model of Federrath et al. (2010), which describes the proportionality parameter b as a function of the turbulent forcing. This model predicts for solenoidal forcing $b = 1/3$ and for compressive forcing $b = 1$. Our measurements agree with the model of Federrath et al. (2010) in the supersonic case for both types of forcing. We see small deviations from the model in the simulations with $\mathcal{M} = 15$, which is caused by our limited resolution (see figure 4). The std. dev.s of the density distribution of the simulation with solenoidal forcing are smaller than the prediction of the model in the subsonic case. In the subsonic regime, the deviations are caused by the thermal pressure, which damps density variations and compressible modes of the velocity field and reduces the measured std. dev. below the model prediction as discussed in section 3.3. The upper right panel of figure 6 shows the mass-weighted, logarithmic std. dev. $\sigma_{s,M}$ as a function of the r.m.s. Mach number. The dotted and dashed-dotted lines correspond to the standard model for the logarithmic density variance,

$$\sigma_s^2 = \ln(1 + b^2 \mathcal{M}^2) \quad (8)$$

with $b = 1/3$ for solenoidal and $b = 1$ for compressive forcing. Equation (8) follows from equations (7) and (1) and was recently derived analytically by Molina et al.

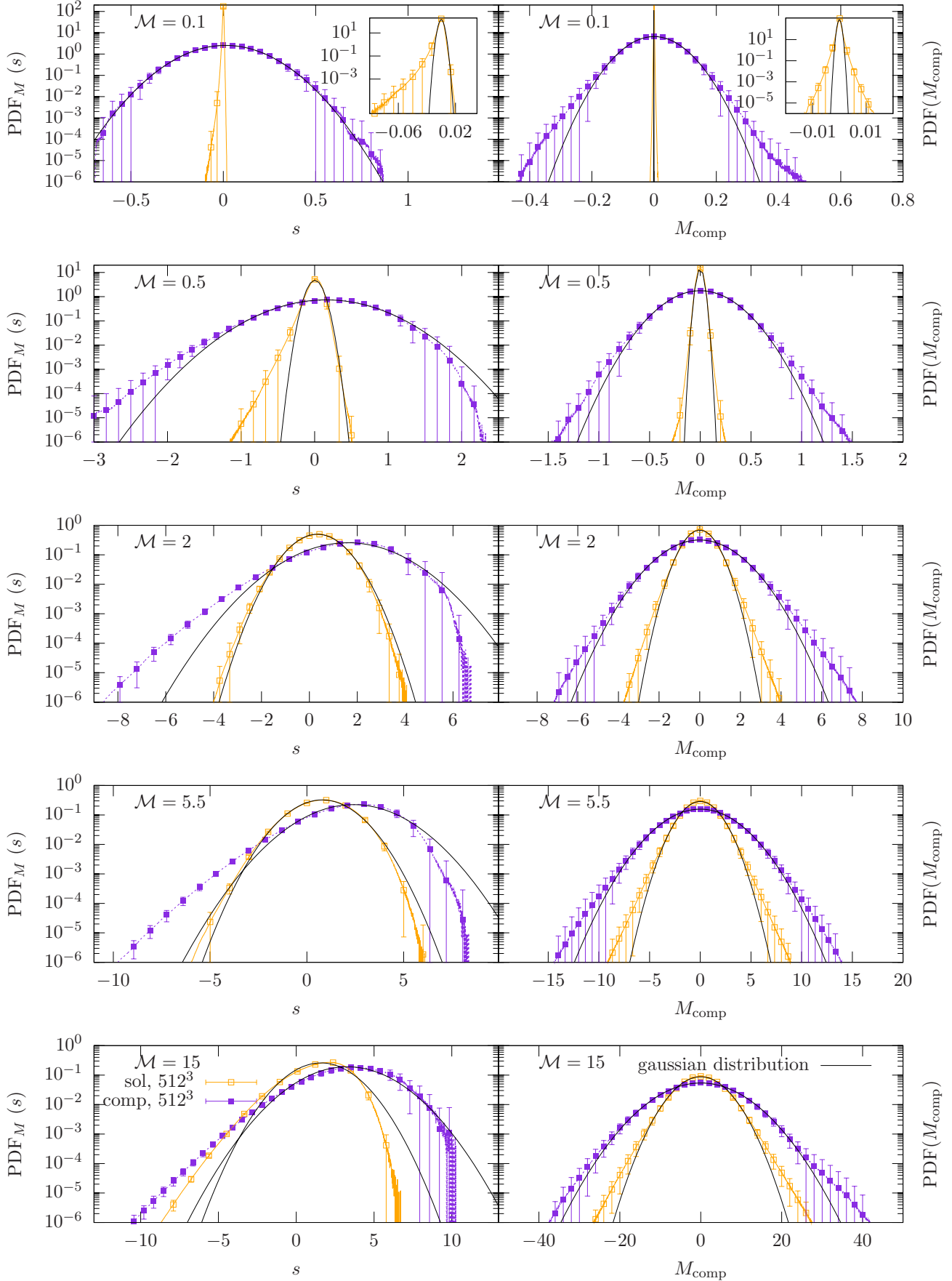


FIG. 5.— The mass-weighted PDFs of the logarithm of the mass density (left panels) and the compressible part of the local Mach number (right panels) for different r.m.s. Mach numbers, resolutions and both types of forcing. In the inset, a magnification of the PDFs obtained with solenoidal forcing for $\mathcal{M} = 0.1$ are shown. The error bars in each panel indicate the std. dev. of the temporal fluctuations.

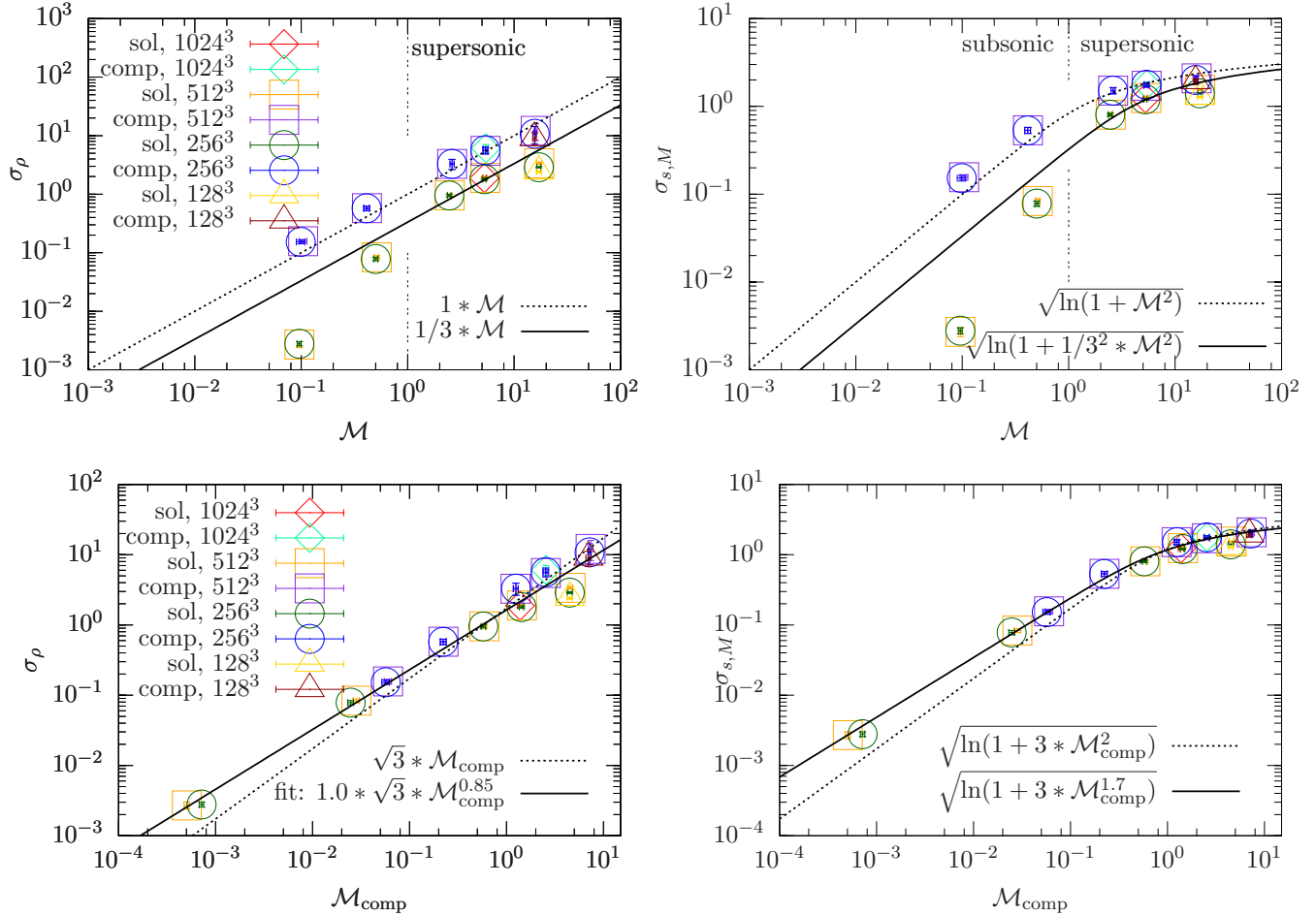


FIG. 6.— The std. dev. of the distribution of the mass density (left) and the std. dev. of the distribution of the logarithm of the mass density (right) as a function of the r.m.s. Mach number (upper panels) and as a function of the compressible part of the r.m.s. Mach number (lower panels). In the upper panels the lines correspond to the model of Federrath et al. (2010) with $b = 1/3$ for solenoidal forcing and $b = 1$ for compressive forcing. In the lower panels the solid lines correspond to a two-parameter fit and the dotted line corresponds to a linear relation between the std. dev. of the mass density and the std. dev. of the compressible part of the r.m.s. Mach number with a proportionality constant $\sqrt{3}$.

(2012) using the shock-jump conditions and averaging over an ensemble of shock waves. The deviations of our numerical data from this standard model are only significant for solenoidal forcing in the subsonic regime, while our data are in excellent agreement with equation (8) for both solenoidal and compressive forcing in the supersonic regime, given our resolution dependence of the $\mathcal{M} = 15$ data points. Our results are in agreement with Kowal et al. (2007), who found deviations from the linear relation with σ_ρ in the subsonic regime with solenoidal forcing, and with Passot & Vázquez-Semadeni (1998), who analysed one-dimensional simulations with only compressive forcing and $0.5 \leq \mathcal{M} \leq 3$ and found the linear relation between \mathcal{M} and σ_ρ with $b = 1$. Price et al. (2011) analysed three dimensional simulations with purely solenoidal forcing and r.m.s. Mach numbers in between $2 \leq \mathcal{M} \leq 20$ and found $b = 1/3$ in excellent agreement with our result. As they did not analyse the subsonic regime with solenoidal forcing they did not observe the large deviations in the subsonic regime. Our analysis complements these studies with measurements in both the subsonic and supersonic regime and for purely compressive forcing.

3.5. Physical origin of density fluctuations in turbulent flows

Studying the continuity equation (2), one can argue that variations of the density can only be caused by the divergence of the velocity field. Given that a vector field can be decomposed in a gradient field and a rotation field and that the divergence of a rotation field vanishes, we conclude that the density variations can only be caused by the compressible modes of the velocity. For this reason we replaced the r.m.s. Mach number, which is in fact the std. dev. of the velocity distribution, with the compressible part of the r.m.s. Mach number, $\mathcal{M}_{\text{comp}}$, in the lower panels of figure 6. The data points show a clear correlation. The different behaviour of the simulations driven with solenoidal and compressive forcing are significantly reduced. We added in figure 6 a function (dotted line) for the relation $\sigma_\rho = \sqrt{3} \mathcal{M}_{\text{comp}}$, which is the simplest model for this relation assuming isotropy. The factor of $\sqrt{3}$ is due to the fact that we use the distribution of the compressible modes of the velocity field averaged over the three directions of the coordinate system

$$\mathcal{M}_{\text{comp}}^{\text{tot}} = \sqrt{\mathcal{M}_{\text{comp},x}^2 + \mathcal{M}_{\text{comp},y}^2 + \mathcal{M}_{\text{comp},z}^2} \quad (9)$$

$$= \sqrt{3} \mathcal{M}_{\text{comp}}.$$

A similar model has also been suggested by Federrath et al. (2010), where the parameter b in equations (1) and (8) was approximated by $\sqrt{D} \langle \Psi \rangle$ with the spatial dimension D of the turbulence ($D = 3$ in our case) and the so-called compressive ratio $\langle \Psi \rangle$, which is the ratio of compressible to total velocity fluctuations. This and our simple model fits the data, but shows deviations for the simulations with solenoidal forcing and the lowest and highest Mach numbers. The deviations for the $\mathcal{M} = 15$ simulation are again caused by the resolution dependency of σ_ρ . Additionally, we perform a fit of our data (black solid line) with two free parameters, $\sigma_\rho = \alpha \sqrt{3} \mathcal{M}_{\text{comp}}^\beta$ for the density relation. We obtain a normalisation $\alpha = 1.0 \pm 0.1$ and a slope $\beta = 0.85 \pm 0.04$. For the s -relation we transform the fitted function with equation (7). The measurements of the std. dev. of the density have larger deviations from the model as the measurements of the std. dev. of s . However, the model fits the measurements in both cases and provides a good description for the data points in the subsonic regime with solenoidal forcing, which are strongly influenced by sound waves. We conclude that the thermal pressure damps the velocities in compressible modes in a way that the relation between the velocities in compressible modes and the density variations in a turbulent medium is in a statistical equilibrium state, even if the medium is strongly influenced by sound waves. The deviation of the scaling exponent from the simple model can be interpreted as additional dissipative effects, which are proportional to $\mathcal{M}_{\text{comp}}$. An example for these physical processes are shocks, which cause deviations from the log-normal distribution of the density PDF. However, systematic errors with a dependency on the r.m.s. Mach number could also cause deviations from the linear scaling and would be another possible interpretation for our fitted scaling exponent. The shown relation between the std. dev. of the density and the compressible part of the r.m.s. Mach number in principle enables us to measure the kinetic energy in compressible modes in giant molecular clouds, without knowing the absolute r.m.s. Mach number, the driving mechanism or the sound speed. The relations shown in the bottom panels of figure 6 are valid in both, the subsonic and supersonic regime.

4. SUMMARY AND CONCLUSIONS

We have investigated the influence of solenoidal (divergence-free) and compressive (curl-free) forcing on the PDF of the mass density in subsonic and supersonic turbulence with a set of three-dimensional numerical simulations. We analysed the relation between the std. dev. of the mass density distribution and the r.m.s. Mach number. We found a new relation between the std. dev. of the mass density and the std. dev. of the compressible part of the velocity field. Our main results are as follows:

- Compressive forcing yields mass density PDFs with std. dev.s proportional to the r.m.s. Mach number with $b = 1$. For solenoidal forcing, we measure $b = 1/3$ in the supersonic regime. Our findings are

in agreement with previous studies, which however only explored different subsets of the full parameter space investigated here. We also found deviations of our measurements from the linear relation with solenoidal forcing in the subsonic regime. These deviations from the linear relation can be explained with sound waves, which damp the faint compressible velocities and prevent the medium from producing over-densities.

- We found a unique relation between the std. dev. of the mass density and the compressible modes of the velocity field with a fit to our data. Our new relation is independent of the driving mechanism and still holds in the subsonic regime, where the flow is mainly influenced by sound waves. It does not show a strong influence on the resolution and other effects, which may cause a non-Gaussian distribution of the density.
- Our relation enables us for the first time to measure the kinetic energy in compressible modes in units of the sound speed, without knowing the r.m.s. Mach number, the driving mechanism or the sound speed of the medium. This measurement can be used to distinguish between subsonic and supersonic compressive turbulent motions. It will in principle allow us to measure the composition of the kinetic energy in the interstellar medium by combining independent measurements of the total r.m.s. Mach number (e.g. Burkhart et al. 2009) and the std. dev. of the density distribution (Brunt et al. 2010; Brunt 2010; Schneider et al. 2012).

L.K. and P.G. acknowledge financial support by the International Max Planck Research School for Astronomy and Cosmic Physics (IMPRS-A) and the Heidelberg Graduate School of Fundamental Physics (HGSFP). The HGSFP is funded by the Excellence Initiative of the German Research Foundation DFG GSC 129/1. L.K., P.G., C.F., and R.S.K. acknowledge subsidies from the Baden-Württemberg-Stiftung via the program *Internationale Spitzenforschung II* (grant P-LS-SPII/18) from the German Bundesministerium für Bildung und Forschung via the ASTRONET project STAR FORMAT (grant 05A09VHA). P.G. acknowledges the support by the Max-Planck Institut für Astrophysik in Garching. C.F. acknowledges funding provided by the Australian Research Council under the Discovery Projects scheme (grant no. DP110102191). R.S.K. furthermore gives thanks for subsidies from the Deutsche Forschungsgemeinschaft (DFG) under grants KL 1358/10, and KL 1358/11 and via the SFB 881 'The Milky Way System', as well as from a Frontier grant of Heidelberg University sponsored by the German Excellence Initiative. Supercomputing time at the Leibniz Rechenzentrum (grant no. h0972 and pr32lo), and at the Forschungszentrum Jülich (grant no. hhd20) are gratefully acknowledged. The software used in this work was in part developed by the DOE-supported ASC / Alliance Center for Astrophysical Thermonuclear Flashes at the University of Chicago.

REFERENCES

- Beetz, A., Gollwitzer, C., Richter, R., & Rehberg, I. 2008, *Journal of Physics Condensed Matter*, 20, 204109
- Brunt, C. M. 2010, *Astronomy and Astrophysics*, 513, A67
- Brunt, C. M., Federrath, C., & Price, D. J. 2010, *Monthly Notices of the Royal Astronomical Society*, 403, 1507
- Burkhart, B., Falceta-Gonçalves, D., Kowal, G., & Lazarian, A. 2009, *The Astrophysical Journal*, 693, 250
- Colella, P., & Woodward, P. R. 1984, *Journal of Computational Physics*, 54, 174
- Dubey, A., Fisher, R., Graziani, C., Jordan, IV, G. C., Lamb, D. Q., Reid, L. B., Rich, P., Sheeler, D., Townsley, D., & Weide, K. 2008, in *Astronomical Society of the Pacific Conference Series*, Vol. 385, *Numerical Modeling of Space Plasma Flows*, ed. N. V. Pogorelov, E. Audit, & G. P. Zank, 145
- Elmegreen, B. G. 2008, *The Astrophysical Journal*, 672, 1006
- Elmegreen, B. G., & Scalo, J. 2004, *Annual Review of Astronomy and Astrophysics*, 42, 211
- Federrath, C., Klessen, R. S., & Schmidt, W. 2008, *The Astrophysical Journal, Letters*, 688, L79
- Federrath, C., Roman-Duval, J., Klessen, R. S., Schmidt, W., & Mac Low, M. 2010, *Astronomy and Astrophysics*, 512, A81
- Fryxell, B., Olson, K., Ricker, P., Timmes, F. X., Zingale, M., Lamb, D. Q., MacNeice, P., Rosner, R., Truran, J. W., & Tufo, H. 2000, *Astronomy and Astrophysics, Supplement*, 131, 273
- Hennebelle, P., & Chabrier, G. 2008, *The Astrophysical Journal*, 684, 395
- . 2009, *The Astrophysical Journal*, 702, 1428
- . 2011, *The Astrophysical Journal, Letters*, 743, L29
- Klessen, R. S. 2000, *The Astrophysical Journal*, 535, 869
- Konstandin, L., Federrath, C., Klessen, R. S., & Schmidt, W. 2012, *Journal of Fluid Mechanics*, 692, 183
- Kowal, G., Lazarian, A., & Beresnyak, A. 2007, *The Astrophysical Journal*, 658, 423
- Kritsuk, A. G., Norman, M. L., Padoan, P., & Wagner, R. 2007, *The Astrophysical Journal*, 665, 416
- Li, Y., Klessen, R. S., & Mac Low, M. 2003, *The Astrophysical Journal*, 592, 975
- Mac Low, M.-M., & Klessen, R. S. 2004, *Reviews of Modern Physics*, 76, 125
- McKee, C. F., & Ostriker, E. C. 2007, *Annual Review of Astronomy and Astrophysics*, 45, 565
- Molina, F. Z., Glover, S. C. O., Federrath, C., & Klessen, R. S. 2012, *ArXiv e-prints-1203.2117*
- Padoan, P., & Nordlund, Å. 2002, *The Astrophysical Journal*, 576, 870
- . 2011, *The Astrophysical Journal*, 730, 40
- Padoan, P., Nordlund, A., & Jones, B. J. T. 1997, *Monthly Notices of the Royal Astronomical Society*, 288, 145
- Passot, T., & Vázquez-Semadeni, E. 1998, *Physical Review E*, 58, 4501
- Passot, T., Vázquez-Semadeni, E. C., & Pouquet, A. 1994, *A turbulent model for the interstellar medium.*, ed. Franco, J., Lizano, S., Aguilar, L., & Daltabuit, E., 246
- Price, D. J., Federrath, C., & Brunt, C. M. 2011, *The Astrophysical Journal, Letters*, 727, L21
- Schmidt, W., Federrath, C., Hupp, M., Kern, S., & Niemeyer, J. C. 2009, *Astronomy and Astrophysics*, 494, 127
- Schneider, N., Csengeri, T., Hennemann, M., Motte, F., Didelon, P., Federrath, C., Bontemps, S., Di Francesco, J., Arzoumanian, D., Minier, V., André, P., Hill, T., Zavagno, A., Nguyen-Luong, Q., Attard, M., Bernard, J.-P., Elia, D., Fallscheer, C., Griffin, M., Kirk, J., Klessen, R., Könyves, V., Martin, P., Men'shchikov, A., Palmeirim, P., Peretto, N., Pestalozzi, M., Russeil, D., Sadavoy, S., Soubie, T., Testi, L., Tremblin, P., Ward-Thompson, D., & White, G. 2012, *Astronomy and Astrophysics*, 540, L11
- Tassis, K. 2007, *Monthly Notices of the Royal Astronomical Society*, 382, 1317
- Vazquez-Semadeni, E. 1994, *The Astrophysical Journal*, 423, 681